Ab-Initio Study of Water Molecule Adsorption on Monoclinic Scheelite-Type $BiVO_4$ Surfaces

Dragan Toprek[a,*], Vasil Koteski[a], Jelena Belošević-Čavor[a], Valentin Ivanovski[a], Ana Umićević[a]

[a]*Department of Nuclear and Plasma Physics, Vinča Institute of Nuclear Sciences - National Institute of the Republic of Serbia, University of Belgrade, P.O Box 522, 11001, Belgrade, Serbia*

Abstract

Herein, we present a study on the adsorption of one water molecule (bonded to either Bi or V sites) and two water molecules (bonded to both Bi and V sites) onto seven low-index surfaces (001), (010), (011), (100), (101), (110), and (111) as well as one high-index surface (211) of a monoclinic scheelite-type $BiVO_4$ crystal structure using ab initio calculations. By predicting the adsorption energies for different facets, we find that water adsorption is more likely to occur on Bi sites. However, for the (001) and (211) surfaces, water adsorption is more likely on the V sites. Furthermore, we find that the studied low-index facets can be grouped into four distinct categories. Facets within the same group exhibit similar water adsorption energies. These groups are ((001)), ((010), (100)), ((110)), and ((011), (101), (111)). For low-index surfaces, favorable adsorption occurs on the (001) surface on the V sites.

Keywords: $BiVO_4$, water adsorption, ab initio calculations, surface energy, adsorption energy

1. Introduction

Hydrogen is an environmentally clean, non-fossil fuel. The production of hydrogen via electrocatalytic and photocatalytic water splitting processes has been widely studied. Bismuth vanadate semiconductor ($BiVO_4$) is one of the materials frequently studied for photoelectrochemical (PEC) water splitting, enabling efficient solar energy conversion to chemical fuels and contributing to environmental protection. $BiVO_4$ is an n-type semiconductor with a bandgap width of 2.3–2.9 eV [1–5]. Using $BiVO_4$, approximately 11% of the solar spectrum can be efficiently converted into chemical fuel. In contrast, the highest percentage of the solar spectrum that can be converted into chemical fuel using other semiconductor oxides is about 8% [6]. Therefore, $BiVO_4$ has attracted the attention of both experimental and theoretical researchers.

$BiVO_4$ has three crystalline phases: monoclinic scheelite-type (ms-$BiVO_4$), tetragonal scheelite-type (ts-$BiVO_4$), and tetragonal zircon-type (tz-$BiVO_4$) [7, 8]. Among them, ms-$BiVO_4$ is stable at ambient temperature and pressure. Herein, we focused on the structure of ms-$BiVO_4$.

The photocatalytic mechanism of $BiVO_4$ can be enhanced by doping it with individual rare earth elements [9–11] or by codoping it with various types of ions [7, 12].

Because water can interact only with the surface of a material, understanding the structure of the hydrated surfaces of that material is important. Similarly, to gain a better understanding of the $BiVO_4$ aqueous electrolyte interfaces used in solar water splitting, it is necessary to study the hydrated surface structure [13]. It has also been shown that surface

*E-mail: toprek@vin.bg.ac.rs

factors, such as orientations and electronic structures, have a crucial impact on the efficiency of photocatalytic activity for $BiVO_4$ [14].

Knowledge of the surface physics and chemistry of $BiVO_4$ is crucial for improving the desired surface physicochemical properties and can help understand and control the catalytic and PEC properties of $BiVO_4$ for widespread applications. One such application is energy conversion and storage [8, 15]. It is well known that some facets exhibit greater reactivity for photocatalysis than others. It is desirable to synthesize crystals with a high percentage of these highly reactive facets. Understanding the relationship between the photocatalytic activity of $BiVO_4$ and the orientation of its surfaces is of great interest for the design and preparation of $BiVO_4$ with high performance and efficiency.

In the study of Kamble and Ling, a significant percentage of the exposed (211) surface has been identified by X-ray diffraction in ms-$BiVO_4$ [16]. Numerous studies have addressed the low-index surfaces of $BiVO_4$ (see, for example, Ref. [8]); however, only a few have investigated the physical and chemical properties of the (211) surface. One of the aims of the present work is to enhance our understanding of the adsorption properties of low-indexed $BiVO_4$ surfaces, including one high-index surface (211).

Herein, we investigated the structures, reactivity, and water adsorption properties of several surfaces of ms-$BiVO_4$ using ab initio calculations. Our study focuses on the dynamics and behavior of H_2O molecules on ms-$BiVO_4$ surfaces. The results of this study will provide a foundation for future work on $BiVO_4$-based materials with enhanced performance and efficiency for solar water splitting.

2. Computational method

$BiVO_4$ prepared in the laboratory crystallizes in a scheelite-type or zircon-type structure [2,16,17,18]. The scheelite-type structure can exhibit either a monoclinic (space group number 15, C2/c setting) or tetragonal (space group number 88, $I4_1/a$ setting) crystal system. Space group number 15 has several different settings, including C2/c, I2/b, I2/a, and B2/b [8].

Herein, we focus on the monoclinic scheelite-type $BiVO_4$ crystal structure, space group number 15, C2/c setting, which is denoted in this work as ms-$BiVO_4$. The calculated lattice parameters a, b, c, α, β and γ of ms-$BiVO_4$ are presented in Table 1 and compared with those from Ref. [19].

The first principles density functional theory (DFT) calculations were performed using the Vienna ab initio simulation package (VASP) code to optimize the crystal structures [20,21]. Optimization is an iterative process in which the total energy of the structure and the atomic forces are minimized by adjusting the coordinates of the atoms and lattice parameters. Plane waves and projector augmented wave pseudopotentials, implemented in the VASP code, were used to calculate the ground state properties of the crystalline structures. The electronic exchange-correlation energy was treated using the generalized gradient approximation parametrized by Perdew–Burke–Ernzerhof [22-24], which underestimates the band gaps. Hybrid exchange-correlation functionals, such as B3LYP or B3PW, achieve excellent agreement with experimental data for the bandgaps of related perovskite materials [25-26]. We selected the Monkhorst-Pack 8 × 8 × 8 k-point mesh (for the pure bulk system) and 4 × 4 × 1 k-point mesh (for the pure surface system) to sample the entire Brillouin zone, yielding 512 points (for the pure bulk system) and 16 points (for the pure surface system) in the irreducible Brillouin zone

[27]. A cut-off energy of 500 eV was chosen. The bulk structure was relaxed according to the Hellmann–Feynman forces calculated at the end of each self-consistent cycle until the forces acting on all atoms were less than 0.02 eV/Å. Self-consistency was achieved by requiring the convergence of the integrated charge difference between the last two iterations to be smaller than 10^{-5} e^{-}. All calculations refer to zero temperature.

3. Results and discussion

3.1. ms-$BiVO_4$ bulk calculations and optimizations

From Table 1, it can be seen that our calculated parameters are in excellent agreement with previous calculations [19]. The optimized ms-$BiVO_4$ structure shown in Fig. 1 was used to calculate the adsorption properties of the facets considered in this study.

Table 1
Calculated lattice parameters of ms-$BiVO_4$. The calculated values from Ref. [19] are presented for comparison. V is the cell volume.

	ms-$BiVO_4$	
	This work	Ref. [19]
***a* [Å]**	6.9026	6.9256
***b* [Å]**	6.9022	6.9256
***c* [Å]**	5.1460	5.1774
α [°]	68.11	68.05
β [°]	68.11	68.05
γ [°]	116.24	116.02
***V* [Å^3]**	155.770	158.134

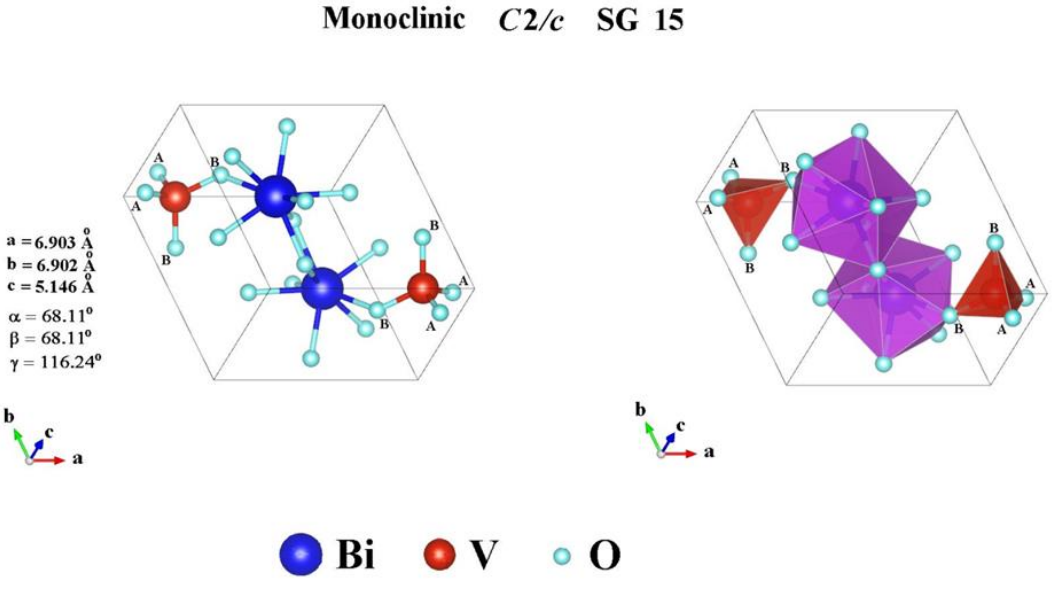

Fig. 1. Calculated ms-$BiVO_4$ structure. The Bi, V, and O atoms are shown in blue, red, and

turquoise, respectively. Some oxygen atoms are labeled A and B (see the text for an explanation). The right side displays the same crystal structure in polyhedral style.

In the $BiVO_4$ structure, the V atom is surrounded by four O atoms, forming a VO_4 tetrahedron (Fig. 2 - left part). Each Bi atom is surrounded by eight O atoms, forming BiO_8 dodecahedrons (Fig. 2 - right part) located at the corners of eight different VO_4 tetrahedra. The ion–ion distances of this crystal structure are shown in Table 2.

The bond lengths of Bi–O, (~2.45 Å, Table 2) are considerably larger than those of V–O (~1.75 Å). Consequently, the interaction between V and O atoms is stronger than that between Bi atoms and O atoms. The same conclusion is drawn in the study reported by Zhao et al. for monoclinic clinobisvanite $BiVO_4$ [14].

In the VO_4 tetrahedron, there are two types of O atoms, labeled "A" and "B" in Figs. 1 and 2. This study, along with the findings of Zhao et al., indicates that the behaviors of these two types of oxygen atoms differ in the surface models [14]. The bond lengths between the V atom and the corresponding "A" and "B" oxygen atoms as well as the angles (<) are as follows:

$$d\,(V–O_A) = 1.741\ Å$$
$$d\,(V–O_B) = 1.759\ Å$$
$$< (O_A–V–O_A) = 115.22^o$$
$$< (O_B–V–O_B) = 117.10^o$$

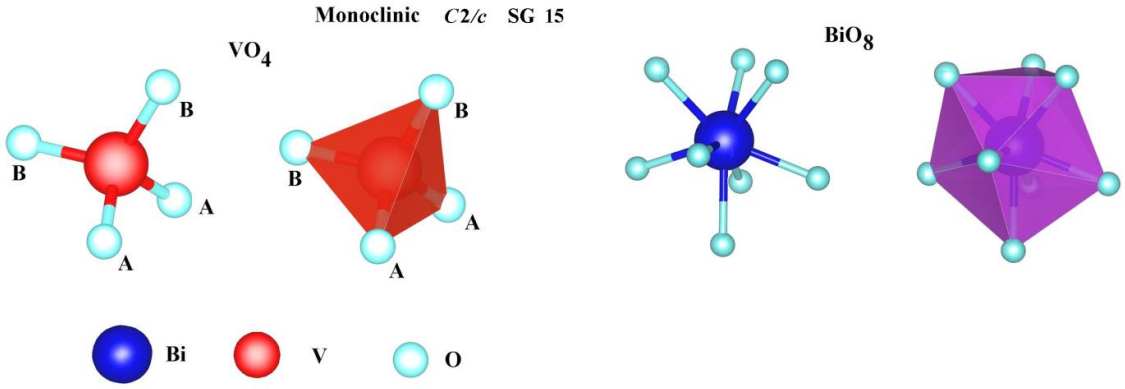

Fig. 2. VO_4 tetrahedron and BiO_8 dodecahedra of ms-$BiVO_4$.

Table 2
Different ion–ion distances of ms-$BiVO_4$. The calculated values from Ref. [19] are provided for comparison.

	ms-$BiVO_4$	
	This work	Ref. [19]
$d_{Bi–Bi}$ **[Å]**	3.873–3.933	3.889–3.948
$d_{V–V}$ **[Å]**	3.866–3.940	3.882–3.955

$d_{Bi–O}$ [Å]	2.418–2.454	2.432–2.463
$d_{V–Bi}$ [Å]	1.741–1.759	1.75–1.768

We also performed a calculation for an isolated water molecule by considering the water molecule in a 30 Å × 30 Å × 30 Å box. The calculated total energy E_W of an isolated water molecule is −14.272 eV, the calculated O–H bond length is 0.972 Å (experimental value is 0.957 Å), and the calculated H–O–H angle is 104.668º (experimental value is 104.52º) [28,29].

3.2. ms-$BiVO_4$ surface structure calculations

The calculated lattice constants for bulk ms-$BiVO_4$ presented in Table 1 are used to construct various facets, as listed in Table 3, from bulk termination. Each ms-$BiVO_4$ surface is represented by a slab with lattice constants a and b, as calculated for the bulk. For the c direction, the slab thickness is chosen such that the lower surface always has a bulk-truncated structure, and a 10 Å vacuum layer is added above the surface of interest. No symmetry is imposed during the relaxation. It should be emphasized that oxygen atoms bound only to bismuth atoms are removed from the facet to the lower layer. In this way, the stoichiometric formula of the crystal structure is maintained, but the facet is cleared of the Bi–O bond [7]. We focus on the Bi–O bond because its strength ($E_{Bi–O}$ = 0.52 eV) is much weaker than that of the V–O bond ($E_{V–O}$ = 3.54 eV) [7]. This is consistent with the conclusion regarding the strength of the interactions between Bi and V atoms with O atoms made in the previous section (3.1) and Ref. [14]. The low-index surfaces (hkl) are modeled using the function [30]:

ase.build.cut (bulk, (A_x,A_y,A_z), (B_x,B_y,B_z), nlayers)

where (A_x,A_y ,A_z) and (B_x, B_y,B_z) are the components of two vectors $\vec{A}$ and $\vec{B}$, respectively, belonging to the corresponding (hkl) plane.

Let the vector $\overrightarrow{n^{(hkl)}}$ be the vector, which is normal to the (hkl) surface. Then, $\overrightarrow{n^{(hkl)}}$ is always normal to the vectors $\vec{A}$ and $\vec{B}$;

$$\overrightarrow{n^{(hkl)}} \cdot \vec{A} = 0 \quad \text{and} \quad \overrightarrow{n^{(hkl)}} \cdot \vec{B} = 0 \tag{1}$$

The coordinates of the vectors $\vec{A}$, $\vec{B}$ and $\overrightarrow{n^{(hkl)}}$ are not unique; however, we have chosen the values provided in Table 3.

Table 3

Coordinates of the vectors $\vec{A}$, $\vec{B}$, and $\overrightarrow{n^{(hkl)}}$ for the given surface (hkl).

Surface (hkl)	$\overrightarrow{n^{(hkl)}}$	$\vec{A}$	$\vec{B}$
(001)	(0,0,1)	(1,0,0)	(0,1,0)
(010)	(0,1,0)	(1,0,0)	(0,0,1)
(011)	(0,1,1)	(1,0,0)	(1,1,−1)
(100)	(1,0,0)	(0,1,0)	(0,0,1)

(101)	(1,0,1)	(0,1,0)	(1,0,−1)
(110)	(1,1,0)	(0,0,1)	(1,−1,0)
(111)	(1,1,1)	(2,−1,−1)	(1,−2,1)
(211)	(2,1,1)	(1,−3,1)	(1,−1,−1)

The surface stabilities of various facets is estimated using the following formula for surface energy σ [31]:

$$\sigma = \frac{E_{tot} - \frac{N_{slab}}{N_{bulk}} \cdot E_{bulk}}{2 \cdot A} \quad (2)$$

where E_{tot} is the total energy of the slab, E_{bulk} is the total energy of the bulk, N_{slab}, and N_{bulk} are the total number of atoms in the slab and the bulk, respectively, and A is the surface area of the x–y plane of the slab.

Applying the upper procedure, we calculated the termination structure of all considered surfaces of ms-$BiVO_4$. After relaxation, all surfaces exhibit a corrugated structure with a characteristic sawtooth-like profile along the b direction. The main feature of the relaxed surfaces is that they consist of VO_m and BiO_n polyhedra, where $m \leq 4$ and $n < 8$. Additionally, the VO_m and BiO_n polyhedra for different surfaces are slightly deformed compared to the VO_4 and BiO_8 polyhedra in the bulk. After 6–7 monoatomic layers, the crystal structure resembles that of the bulk, consisting of VO_4 and BiO_8 polyhedra. We denote BiO_n polyhedra as Bi_n. The bond lengths and the corresponding angles between the V (Bi) and O atoms located at the corners of the polyhedra are represented by $d_{V–O}$ and $d_{Bi–O}$ and the angles between the O–V–O atoms are denoted as < (O–V–O). These details are presented in Table 4. In Table 4, the first line in the last two columns corresponds to the first Bi monoatomic layer, and the second line corresponds to the second Bi monoatomic layer. The stoichiometric relaxed termination of various facets of ms-$BiVO_4$ is shown in Fig. 3.

Table 4
ms-$BiVO_4$ relaxed surfaces. The bond length, $d_{V–O}$, refers to the distance between the V atom and the O atoms located at the corners of the VO_m polyhedra, while the bond length, $d_{Bi–O}$, refers to the distance between the Bi atom and the O atoms situated at the corners of the BiO_n polyhedra. The angles, < (O–V–O), represent the angles between the O–V–O atoms of the VO_m polyhedra. m and n denote the numbers of oxygen atoms in the VO_m and BiO_n polyhedra, respectively. The first line in the last two columns corresponds to the first Bi monoatomic layer, while the second line corresponds to the second Bi monoatomic layer.

ms-$BiVO_4$					
facet	VO_m			BiO_n	
	m	$d_{V–O}$ [Å]	<(O–V–O) [°]	n	$d_{Bi–O}$ [Å]
(001)	4	1.702–1.856	97.55–128.53	4	2.067–2.500
				5	2.211–2.626
(010)	4	1.619–1.817	94.86–116.23	6	2.261–2.590
(011)	4	1.697–1.799	106.50–112.30	5	2.175–2.417
(100)	4	1.619–1.817	101.30–116.31	6	2.260–2.592
				7	2.236–2.617

(101)	4	1.621–1.819	94.80–115.86	6	2.246–2.617
				7	2.239–2.588
(110)	3	1.736–1.806	113.45–130.85	4	2.109–2.517
(111)	4	1.660–1.791	104.97–115.36	3	2.101–2.187
				5	2.218–2.538
(211)	3	1.638–1.750	104.75–110.93	4	2.182–2.348
				5	2.085–2.626

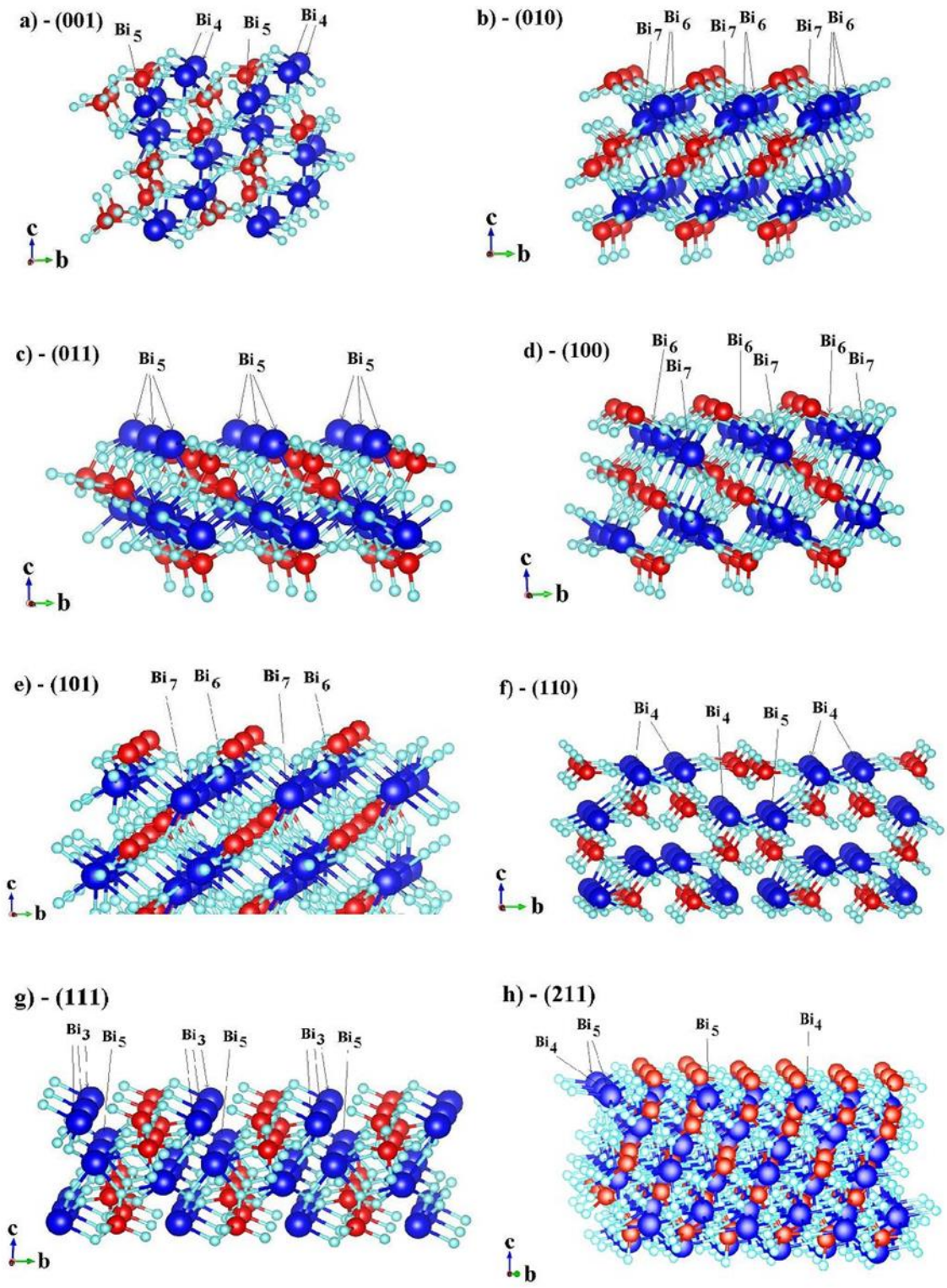

Fig. 3. Structure of the relaxed surfaces of ms-$BiVO_4$.

The calculated ms-$BiVO_4$ surface energies and other parameters from Eq. 2 are listed in Table 5. The numbers in brackets represent results from Ref. [8] and Ref. [31]. In Ref. [8], the authors examined the same crystal structure but in a different setting, I2/b, referred to as the Ferguson-type monoclinic (fm-$BiVO_4$; see Table 1 in Ref. [8]). In Ref. [31], the authors analyzed the anatase TiO_2 crystal structure.

Table 5
Unit cell parameters a, b, and α, the number of atoms N_{slab} in the slab, the area of the surface unit cell A, the relaxed total energy E_{tot} of the slab, and the relaxed surface energy σ for different facets of ms-$BiVO_4$. The numbers in brackets are results from (a) Ref. [8] and (b) Ref. [31].

ms-$BiVO_4$					
		***N_{bulk}* = 12, *E_{bulk}* = −88.917 eV**			
facet	N_{slab}	Unit cell param. [Å]	A [Å^2]	E_{tot} [eV]	σ [J/m^2]
(001)	36	a = 6.903 b = 6.902 α = 116.2°	42.75	−262.838	0.733 (0.57)[a] (1.08)[b]
(010)	24	a = 6.903 b = 5.146 α = 68.1°	32.96	−175.594	0.544 (0.31)[a]
(011)	18	a = 6.903 b = 5.164 α = 68.0°	33.05	−131.444	0.468 (0.49)[a]
(100)	24	a = 6.902 b = 5.146 α = 68.1°	32.96	−175.594	0.544 (0.63)[a]
(101)	54	a = 6.902 b = 6.902 α = 136.1°	34.33	−399.019	0.258 (0.62)[a] (0.52)[b]
(110)	72	a = 5.146 b = 11.723 α = 90°	60.33	−515.992	2.325 (0.35)[a] (1.15)[b]
(111)	24	a = 6.902 b = 6.902 α = 116.2°	42.73	−174.844	0.561 (0.34)[a]
(211)	108	a = 24.007 b = 12.802 α = 26.6°	137.61	−784.484	0.918 (0.97)[b]

3.3. Water adsorption on ms-$BiVO_4$ surfaces

The adsorption of an isolated water molecule on ms-$BiVO_4$ with different facets was investigated by considering three adsorption configurations: (a) one water molecule adsorbed on a single surface Bi atom (denoted as Bi_nW, see the fourth column of Table 6), where Bi_n represents the polyhedron for the corresponding facet (Section 3.2); (b) one water molecule adsorbed on a surface V atom (denoted as VW in Table 6); and (c) two water molecules adsorbed on both the surface V and Bi atoms (denoted as Bi_nVW in Table 6). Surface atoms are defined as those located at the topmost layer of the surface unit cell. For each adsorption configuration, the water molecules are positioned upright on the top sites. We optimized these

structures, and the results are shown in Fig. 4 and Tables 6–9 after relaxation of each configuration.

Table 6
Relaxation adsorption energy E_{ads} per water molecule, total energy E_{tot} in the absence of water molecules, total energy of the isolated water molecule E_W, number of water molecules N_W adsorbed on the surface, and total energy of the relaxed system with water molecules E_{all} are reported for different facets of ms-$BiVO_4$. The bold numbers for the relaxed adsorption energies represent the highest values, but only in the case when one water molecule is considered (adsorbed configuration (a) or (b) in Section 3.3).

ms-$BiVO_4$					
facet	N_W	E_{tot} [eV]	E_W = −14.272 eV adsorb. configur. (before relax.)	E_{all} [eV]	E_{ads} [eV]
(001)	1	−262.838	Bi_4W	−278.399	1.289
	1		VW	−279.351	**2.241**
	2		Bi_4VW	−293.350	0.984
(010)	1	−175.594	Bi_6W	−191.208	**1.342**
	1		VW	−190.341	0.474
	2		Bi_6VW	−205.943	0.903
(011)	1	−131.444	Bi_5W	−146.366	0.650
	1		VW	−146.550	**0.834**
	2		Bi_5VW	−161.317	0.665
(100)	1	−175.594	VW	−190.615	0.749
	1		Bi_6W	−191.207	**1.341**
	1		Bi_7W	−190.559	0.693
	2		Bi_6VW	−202.187	−0.976
(101)	1	−399.019	Bi_6W	−413.965	**0.674**
	1		VW	−413.578	0.287
	2		Bi_6VW	−429.070	0.753
(110)	1	−515.992	Bi_4W	−530.963	0.699
	1		Bi_4W	−531.345	**1.081**
	1		VW	−531.234	0.970
	2		Bi_4VW	−550.048	2.756
(111)	1	−174.844	Bi_3W	−189.808	0.692
	1		VW	−189.971	**0.855**
	2		Bi_3VW	−204.728	0.669
(211)	1	−784.484	VW	−804.291	**5.535**
	11		VW	−954.446	1.179

The relaxation adsorption energy (E_{ads}) of a single water molecule was estimated using the following formula: [32]

$$E_{ads} = \frac{(E_{tot} + N_W \cdot E_W) - E_{all}}{N_W} \quad (3)$$

where E_{tot} is the relaxed total energy of the slab in the absence of water molecules (Tables 5 and 6), E_W is the total energy of the isolated water molecule, N_W is the number of water molecules adsorbed on the surface, and E_{all} is the total energy of the relaxed system with adsorbed water molecules.

For cases (a) and (b) of the adsorption configurations with $N_w = 1$, and for case (c) with $N_w = 2$, according to the definition of adsorption energy (E_{ads}) given by Eq. 3, adsorption is more stable at higher adsorption energies.

In Table 6, the bold numbers for the relaxed adsorption energies represent the highest values, but this applies only when one water molecule is considered (adsorbed configurations (a) or (b)). Table 7 summarizes our results for relaxed ms-$BiVO_4$ surfaces. Table 8 shows the O–H distance (d_{O-H}) and the H–O–H angle (< (H–O–H)) of the adsorbed H_2O molecule for each facet of ms-$BiVO_4$ are shown.

The main characteristic of the unit cell of the relaxed surfaces is that it consists of VO_4 and BiO_4 (labeled Bi_4) polyhedra for surfaces (001) and (110) (Figs. 3a and 3f); VO_4 and BiO_6 (marked by letter Bi_6) polyhedra for surfaces (010), (100) and (101) (Figs. 3b, 3d, and 3e); of VO_4 and BiO_5 (labeled Bi_5) polyhedra for surface (011) (Fig. 3c); and of VO_4 and BiO_3 (labeled Bi_3) polyhedra for surface (111) (Fig. 3g). The main characteristic of the unit cell of the relaxed (211) surface is that it consists of one VO_3 polyhedron (Fig. 3h).

From Table 7, it can be seen that the adsorption on the (001) surface is more stable when the water molecule is adsorbed on the V site (Fig. 4a). In this case of water adsorption, the water molecule is dissociated. V–O and O–H are the distances between corresponding atoms (Fig. 4). The O–H distance of the adsorbed H_2O molecule for the (001) facet is 0.989 Å (Table 8), slightly larger than that of the isolated water molecule (0.972 Å).

Table 7
Relaxed adsorption energy E_{ads} of the water molecule on the different facets of ms-$BiVO_4$. The dissociation of the water molecule occurs when it is adsorbed on the V site.

	ms-$BiVO_4$		
facet	atom site	E_{ads} [eV]	dissociation of water
(001)	V	2.241	YES
(010)	Bi	1.342	NO
(011)	Bi	0.834	NO
(100)	Bi	1.341	NO
(101)	Bi	0.674	NO
(110)	Bi	1.081	NO
(111)	Bi	0.855	NO
(211)	V	5.535	YES

The adsorption on the (010) surface is more stable when the water molecule is adsorbed at the Bi site (Fig. 4b). In this case, the water adsorption is molecular, without dissociation. Bi–O and O–H are the distances between the corresponding atoms (Fig. 4b). The O–H distances and H–O–H angle of the adsorbed H_2O molecule for the (010) facet are 1.006 Å, 1.013 Å, and 108.88° (Table 8), respectively, which are slightly larger than those of an isolated water molecule (0.972 Å, 104.67°). The adsorbed water molecules are stretched due to their hydrogen-bonding interactions [28, 29].

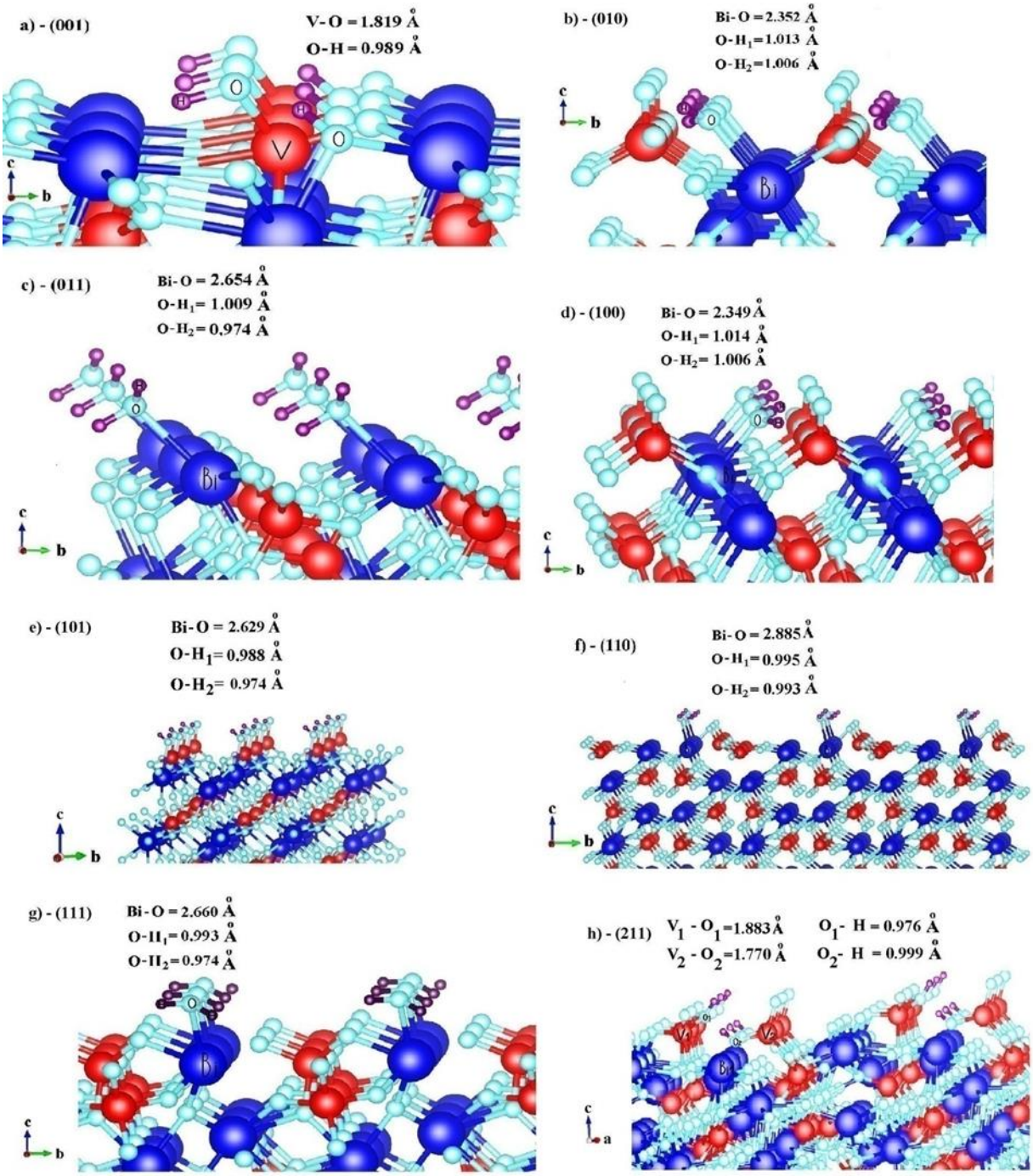

Fig. 4. Optimized structure of adsorbed water molecules on different surfaces of ms-$BiVO_4$.

Similarly, Table 7 shows that water adsorption on the (010), (011), (100), (101), (110), and (111) surfaces is more stable when the water molecule is adsorbed on the Bi site (Figs. 4 b–

g), and there is no dissociation of the water molecule. Bi–O and O–H refer to the distances between the corresponding atoms (Figs. 4 b–g).

The O–H distances and H–O–H angles of the adsorbed H_2O molecules for these facets, as presented in Table 8, are slightly larger than those of the isolated water molecules (0.972 Å, 104.67°). The adsorbed water molecules are stretched due to their hydrogen-bonding interactions [28, 29].

Table 8
O–H distance ($d_{O–H}$) and H–O–H angle (< (H–O–H)) of the adsorbed H_2O molecule for each facet of ms-$BiVO_4$.

ms-$BiVO_4$			
facet	atom site	O–H (Å)	<(H–O–H)
(001)	V	0.989	dehydrized
(010)	Bi	1.006	108.88°
		1.013	
(011)	Bi	0.974	105.52°
		1.009	
(100)	Bi	1.006	108.95°
		1.014	
(101)	Bi	0.974	107.95°
		0.988	
(110)	Bi	0.993	106.01°
		0.995	
(111)	Bi	0.974	107.17°
		0.993	
(211)	V	0.999	dehydrized

In the case of the (211) surface, the water molecule can only be adsorbed on V sites (Table 7). The adsorption energies for scenarios in which 1 and 11 molecules of water are adsorbed are presented in Table 6. In both cases, the water is dissociated. The case of one molecule of water adsorption is shown in Fig. 4h.

From the calculated adsorption energies of the different facets, we can conclude that water adsorption is more favorable on Bi sites in most cases. Only for the (001) and (211) surfaces is water adsorption more favorable on V sites, but this could be a consequence of not accounting for the appropriate surface charges on these surfaces. Additionally, when adsorption is more favorable on V sites, the adsorption energy is higher than in any case on Bi sites.

The adsorption energies of water molecules on the investigated surfaces increased in the following order:

$$\overbrace{\underbrace{(101) < (011) < (111) < (110) < (100) < (010)}_{no\ dissociation}}^{Bi\ site} \overbrace{\underbrace{< (001) < (211)}_{dissociation}}^{V\ site}$$

Table 8 shows that the O–H distance and the H–O–H angle are reduced after adsorption onto the surface compared with the free H_2O molecule. Water molecules are stretched due to their hydrogen-bonding interactions [28, 29].

From Table 7, it is evident that some facets have similar values for the adsorption energies of water molecules, E_{ads}. We will refer to these facets as "equivalent" facets (Table 9). For the ms-$BiVO_4$ crystal system, there are four groups of "equivalent" low-indexed facets (Table 9).

This is particularly interesting for the (011) and (111) facets: even when a water molecule attempts to adsorb on the surface V atom, it will, after relaxation, shift and adsorb to the surface Bi atom.

Table 9
Water molecule adsorption energies, E_{ads}, for the four groups of "equivalent" low-indexed facets ms-$BiVO_4$ and one high-index facet (211).

ms-$BiVO_4$		
facet	atom site	E_{ads} [eV]
(211)	V	5.535
(001)	V	2.241
(010)	Bi	1.342
(100)	Bi	1.341
(110)	Bi	1.081
(111)	Bi	0.855
(011)	Bi	0.834
(101)	Bi	0.674

4. Conclusion

Compared to other common crystalline $BiVO_4$ phases, the monoclinic scheelite-type $BiVO_4$ exhibits superior characteristics regarding visible light adsorption. It is also an efficient material for photocatalytic water splitting. Due to its promising technological applications, it is important to gain in-depth knowledge of the energetics as well as the structural and electronic properties of its surfaces. Based on DFT calculations, we investigated the competition among the most prevalent surface types and the mechanisms of water adsorption.

We found that the most stable surface of monoclinic scheelite-type $BiVO_4$ is the (101) surface. This differs from the alternative characterization of monoclinic $BiVO_4$, where the most stable surface is the (001) surface, while the (101) surface exhibits a somewhat higher surface energy (Ref. [8]). Our results indicate that there are several mechanisms of water adsorption, including molecular and dissociative adsorption. Different adsorption sites are favored depending on the surface type. In general, the Bi surface sites tend to adsorb molecular water, while water molecules are adsorbed dissociatively on the V sites. The most stable (101) surface is the least likely to absorb water, while dissociative water has the highest energy adsorption on the higher index (211) surface.

Therefore, the calculated adsorption energies of the water molecules on the investigated surfaces increased in the order (101) < (011) < (111) < (110) < (100) < (010) < (001) < (211). In

case of low-index surfaces, a favorable adsorption process occurs on the (001) surface at V sites. On the (211) surface, water adsorption is also more likely on the V sites. For all other investigated surfaces, water adsorption is more likely on the Bi sites. For facets (011) and (111), when a water molecule attempts to adsorb onto a surface V atom, it will, after relaxation, move and adsorb onto a surface Bi atom.

Although using a layer of water molecules and accurately estimating the point of zero charge (PZC) are necessary for a realistic comparison of water adsorption on different surfaces, this is a challenging task. Because PZCs vary across surfaces, such an approach requires demanding molecular simulations with a layer of explicit water molecules, which is beyond the scope of this paper. Expanding our research to incorporate the analysis of surface charge and pH of water solutions [33] is a potential future research direction that is needed.

Acknowledgements

The authors acknowledge funding from the Ministry of Science, Technological Development, and Innovation of the Republic of Serbia provided by the Vinča Institute of Nuclear Sciences (Contract No. 451-03-66/2024-03/ 200017). This research was also supported by the Science Fund of the Republic of Serbia, the Program PRISMA, #7377, Water pollutants detection by ZnO-modified electrochemical sensors: From computational modeling via electrochemical testing to real system application - WaPoDe.

Data availability

The raw/processed data required to reproduce these findings can be obtained from the authors upon reasonable request.

References

[1] D. Toprek, V. Koteski, Improving the photocatalytic activity of tetragonal $BiVO_4$ with zircon-type structure through W doping; *Ab initio* calculations, Mater. Chem. Phys. 264 (2021) 124439. https://doi.org/10.1016/j.matchemphys.2021.124439

[2] S. Tokunaga, H. Kato, A. Kudo, Selective Preparation of Monoclinic and Tetragonal $BiVO_4$ with Scheelite Structure and Their Photocatalytic Properties, Chem. Mater. 13 (2001**)** 4624-4628. https://doi.org/10.1021/cm0103390

[3] K. E. Kweon, G. S. Hwang, Hybrid density functional study of the structural, bonding, and electronic properties of bismuth vanadate, Phys. Rev. B 86 (2012) 165209. https://doi.org/10.1103/PhysRevB.86.165209

[4] X. Zhang, Z. Ai, F. Jia, L. Zhang, X. Fan, Z. Zou, Selective synthesis and visible-light photocatalytic activities of $BiVO_4$ with different crystalline phases, J. Mat. Chem. Phys. 103 (2007) 162-167. https://doi.org/10.1016/j.matchemphys.2007.02.008

[5] T. Liu, X. Zhang, J. Guan, C. Richard, A. Catlow, A. Walsh, A. A. Sokol, J. Buckeridge, Insight into the Fergusonite–Scheelite Phase Transition of ABO_4-Type Oxides by Density

Functional Theory: A Case Study of the Subtleties of the Ground State of $BiVO_4$, Chem. Mater. 34 (2022) 5334-5343. https://doi.org/10.1021/acs.chemmater.1c04417

[6] M. Favaro, R. Uecker, S. Nappini, I. Píš, E. Magnano, H. Bluhm, R. van de Krol, D. E. Starr, Chemical, Structural, and Electronic Characterization of the (010) Surface of Single Crystalline Bismuth Vanadate, J. Phys. Chem. C 123 (2019) 8347-8359. https://doi.org/10.1021/acs.jpcc.8b09016

[7] T. Liu, G. Tan, C. Zhao, C. Xu, Y. Su, Y. Wang, H. Ren, A. Xia, D. Shao, S. Yan, Enhanced photocatalytic mechanism of the Nd-Er co-doped tetragonal $BiVO_4$ photocatalysts, Appl. Catal. B 213 (2017) 87-96. http://dx.doi.org/10.1016/j.apcatb.2017.05.018

[8] G-Ling Li, First-principles investigation of the surface properties of fergusonite-type monoclinic $BiVO_4$photocatalyst, RSC Adv. 7 (2017) 9130-9140. https://doi.org/10.1039/C6RA28006D

[9] Y. Luo, G. Tan, G. Dong, L. Zhang, J. Huang, W. Yang, C. Zhao, H. Ren, Structural transformation of Sm^{3+} doped $BiVO_4$ with high photocatalytic activity under simulated sun-light, Appl. Surf. Sci. 324 (2015) 505-511. https://dx.doi.org/10.1016/j.apsusc.2014.10.168

[10] Q. Li, Z. Kang, L. Guo, J. Hu, J. Pan, Sulfur doping improves the weak adsorption on $BiVO_4$ (0 1 0) facet to enhance the oxygen evolution performance, J. Electroanal. Chem. 941 (2023) 117520. https://doi.org/10.1016/j.jelechem.2023.117520

[11] C. Regmi, Y. K. Kshetri, Tae-Ho Kim, R. P. Pandey, S. W. Lee, Visible-light-induced Fe-doped BiVO4 photocatalyst for contaminated water treatment, Mol.Catal.432 (2017) 220-231. https://dx.doi.org/10.1016/j.mcat.2017.02.004

[12] L. Francas, S. Selim, S. Corby, D. Lee, C. A. Mesa, E. Pastor, K-S. Choi, J. R. Durrant, Water oxidation kinetics of nanoporous BiVO4 photoanodes functionalized with nickel/iron oxyhydroxide electrocatalysts, Chem. Sci. 12 (2021) 7442-7452. https://doi.org/10.1039/D0SC06429G

[13] Y. Hermans, S. Murcia-López, A. Klein, W. Jaegermann, BiVO4 Surface Reduction upon Water Adsorption, ACS Energy Lett.4 (2019) 2522-2528. https://doi.org/10.1021/acsenergylett.9b01667

[14] Z. Zhao, Z. Li, Z. Zou, Structure and energetics of low-index stoichiometric monoclinic clinobisvanite BiVO4 surfaces, RSC Adv.1 (2011) 874-883. https://doi.org/10.1039/C1RA00301A

[15] G. Liu, J. C. Yu, G. Q. Lu,–H-M. Cheng, Crystal facet engineering of semiconductor photocatalysts: motivations, advances and unique properties, Chem. Commun. 47 (2011) 6763-6783. https://doi.org/10.1039/C1CC10665A

[16] G. S. Kamble, Y.-C. Ling, Solvothermal synthesis offacet-dependent $BiVO_4$ photocatalyst with enhanced visible-light-driven photocatalytic degradation oforganic pollutant: assessment oftoxicitybyzebrafish embryo, Sci. Rep. 10 (2020) 12993. https://doi.org/10.1038/s41598-020-69706-4

[17] R. S. Roth, J. L. Waring, Synthesis and stability of bismuthotantalite, stibiotantalite, and chemically similar ABO4 compounds, Am. Mineral. 48 (1963) 1348-1356.

[18] Y. Park, K. J. McDonald, K.-S. Choi, Progress in bismuth vanadate photoanodes for use in solar water oxidation, Chem. Soc. Rev. 42 (2013) 2321-2337. https://doi.org/10.1039/C2CS35260E

[19] Materials project: mp-23506. https://legacy.materialsproject.org/materials/mp-23506/.

[20] G. Kresse, J. Furthmüller, Efficient iterative schemes for ab initio total-energy calculations using a plane-wave basis set, Phys. Rev. B 54 (1996) 11169-11186. https://doi.org/10.1103/PhysRevB.54.11169.

[21] G. Kresse, D. Joubert, From ultrasoftpseudopotentials to the projector augmentedwave method, Phys. Rev. B 59 (1999) 1758-1775. https://doi.org/10.1103/PhysRevB.59.1758

[22] J.P.Perdew, K. Burke, M.Ernzerhof, Generalized Gradient Approximation Made Simple, Phys.Rev.Lett. 77 (1996) 3865-3868. https://doi.org/10.1103/PhysRevLett.77.3865

[23] J. P. Perdew, K. Burke, M. Ernzerhof, Generalized Gradient Approximation Made Simple [Phys. Rev. Lett. 77, 3865-3868 (1996)], Phys. Rev. Lett. 78 (1997) 1396-1396. https://doi.org/10.1103/PhysRevLett.78.1396

[24] Y. Zhang, W. Yang, Comment on "Generalized Gradient Approximation Made Simple", Phys.Rev.Lett. 80 (1998) 890-890. https://doi.org/10.1103/PhysRevLett.80.890

[25] R.I. Eglitis and R. Jia, Review of Systematic Tendencies in (001), (011) and (111) Surfaces Using B3PW as well as B3LYP Computations of BaTiO3, CaTiO3, PbTiO3, SrTiO3, BaZrO3, CaZrO3, PbZrO3 and SrZrO3 Perovskites, Materials 16 (2023) 7623. https://doi.org/10.3390/ma16247623

[26] R. I. Eglitis and A.I. Popov, Systematic trends in (001) surface ab initio calculations of ABO3 perovskites, J. Saudi Chem. Soc. 22 (2018) 459-468. https://doi.org/10.1016/j.jscs.2017.05.011

[27] H.J. Monkhorst, J.D. Pack, Special points for Brillouin-zone integrations, Phys. Rev. B 13 (1976) 5188-5192. https://doi.org/10.1103/PhysRevB.13.5188

[28] P.A. Thiel, T. E. Madey, The interaction of water with solid surfaces: Fundamental aspects, Surf. Sci. Rep. 7 (1987) 211-385. https://doi.org/10.1016/0167-5729(87)90001-X

[29] S.Meng, E. G. Wang, S.Gao, Water adsorption on metal surfaces: A general picture from density functional theory studies, Phys. Rev. B 69 (2004) 195404. https://doi.org/10.1103/PhysRevB.69.195404

[30] A. H. Larsen, J. J. Mortensen, J. Blomqvist, I. E. Castelli, R. Christensen, M. Dulak, J. Friis, M. N. Groves, B. Hammer, C. Hargus, E. D. Hermes, P. C. Jennings, P. B. Jensen, J. Kermode, J. R. Kitchin, E. L. Kolsbjerg, J. Kubal, K. Kaasbjerg, S. Lysgaard, J. B. Maronsson, T. Maxson, T. Olsen, L. Pastewka, A. Peterson, C. Rostgaard, J. Schiøtz, O. Sch¨utt, M. Strange, K. S. Thygesen, T. Vegge, L. Vilhelmsen, M. Walter, Z. Zeng, K. W. Jacobsen, The atomic simulation environment - a Python library for working with atoms, J. Phys Condens. Matter 29 (27) (2017) 273002. https://dx.doi.org/10.1088/1361-648X/aa680e

[31] J. Xu, L.-F.Xu, Z.-Z. Li, J.-T. Wang, Z.-S. Lin, K. Liu, Y.-G. Cao, A.Selloni, *Ab Initio* Study of Water Adsorption and Reactivity on the (211) Surface of AnataseTiO_2, Phys. Rev. Appl. 5 (2016) 064001. https://doi.org/10.1103/PhysRevApplied.5.064001

[32] M. Oshikiri, M. Boero, Water Molecule Adsorption Properties on the $BiVO_4$ (100) Surface, J. Phys. Chem. B 110 (2006) 9188-9194. https://doi.org/10.1021/jp0555100

[33] F. Ambrosio, J. Wiktor, A. Pasquarello, pH-Dependent Catalytic Reaction Pathway for Water Splitting at the $BiVO_4$–Water Interface from the Band Alignment, ACS Energy Lett. 3 (2018) 829-834. https://doi.org/10.1021/acsenergylett.8b00104